

Deep transmission of Laguerre–Gaussian vortex beams through turbid scattering media

W. B. WANG,¹ RICHARD GOZALI,¹ LINGYAN SHI,^{1,2} LUKAS LINDWASSER,¹ AND R. R. ALFANO^{1,*}

¹Institute for Ultrafast Spectroscopy and Lasers, Department of Physics, The City College of the City University of New York, 160 Convent Avenue, New York, New York 10031, USA

²Department of Biology, The City College of the City University of New York, 160 Convent Avenue, New York, New York 10031, USA

*Corresponding author: ralfano@ccny.cuny.edu

Received 1 December 2015; revised 28 March 2016; accepted 2 April 2016; posted 4 April 2016 (Doc. ID 254581); published 27 April 2016

Light scattering and transmission of Gaussian (*G*) and Laguerre–Gaussian (LG) vortex beams with different orbital angular momentum (*L*) in various turbid media were investigated. Transmittance was measured with varied ratios of sample thickness (*z*) to scattering mean free path (*l_s*) of turbid media, *z/l_s*. In the ballistic region, the LG and *G* beams were found to have no significant difference on transmittance, while in the diffusive region, the LG beams showed a higher received signal than the *G* beams, and the LG beams with higher *L* values showed a higher received signal than those with lower *L* values. The transition points from ballistic to diffusive regions for different scattering media were determined. This newly observed transmittance difference of LG and *G* beams may be used for deep target detection in turbid media through LG beam imaging. © 2016 Optical Society of America

OCIS codes: (050.1950) Diffraction gratings; (050.4865) Optical vortices; (290.4210) Multiple scattering; (290.7050) Turbid media.
<http://dx.doi.org/10.1364/OL.41.002069>

Laguerre–Gaussian (LG) optical beams possess orbital angular momentum (OAM) due to the vortex phase of $\exp(iL\phi)$. Over the past decade, the properties of optical vortex beams propagating through free space and scattering media have been investigated, and their phase singularities and optical vortices have been revealed [1–5]. The complex LG beams and vector beams add new dimensions to light’s spatial degrees of freedom and properties for light propagation. These include helical shaped and twisted wave fronts, singularities in electronic fields, and spatial vector polarization states of beam profiles. The twisted special light forms open a new renaissance era in optics called “complex vector light.” Wide applications of LG beams include trapping particles, space or fiber communication, imaging and medical diagnosis, micro-machines, spintronics, and quantum information. For these applications, it is of great interest to reveal the influence of the topological charge *L* of vortex beams to their propagation and penetration capabilities through the turbid media.

The Laguerre–Gaussian modes are a natural solution of the paraxial wave equation in cylindrical coordinates. The

amplitude of the complex electric field for an LG beam can be found by solving the paraxial Helmholtz equation. The complex electric field amplitude for an LG beam can be written using the Laguerre polynomial as [2]

$$E(r, \phi, z) = \frac{C_{LP}^{LG}}{\omega(z)} \left(\frac{r\sqrt{2}}{\omega(z)} \right)^{|L|} \exp\left(-\frac{r^2}{\omega^2(z)}\right) \times L_p^{|L|} \left(\frac{2r^2}{\omega^2(z)} \right) \exp\left(-ik\frac{r^2}{2R(z)}\right) * \exp(iL\phi) \exp[i(2p + |L| + 1)\xi(z)], \quad (1)$$

where *r* is the radial distance from the center axis of the beam, *z* is the axial distance from the beam’s narrowest point, *i* is the imaginary unit, $k = 2\pi/\lambda$ is the wave number, $\omega(z)$ is the beam width as a function of *z*, $R(z)$ is the radius of curvature of the beam’s wavefront, $\xi(z)$ is the Gouy phase shift, L_p^L are the generalized Laguerre polynomials, *p* is the radial index ($p \geq 0$), *L* is the azimuthal index (known as the helical phase winding number or topological charge), and C_{LP}^{LG} is an appropriate normalization constant. The lowest-order solution of LG modes ($p = 0, L = 0$) describes a Gaussian (*G*) beam, while higher-order solutions describe higher-order transverse LG beams.

The major differences between LG and *G* beams are as follows: (1) LG beams possess the vortex phase of $\exp(iL\phi)$ as shown by the additional term involving topological charges *L* in Eq. (1); (2) LG beams have the helical and twisted wavefronts as indicated by the phase term in Eq. (1); (3) LG beams have donut shapes and their central areas are dark; and (4) the size of the vortex of a LG beam is determined by the term r^L . These differences may affect the scattering and propagation properties of LG beams in the turbid media in comparison with *G* beams.

In this study, light scattering and transmission of LG vortex beams with different OAM states in turbid media consisting of large or small scattering particles in water were investigated in comparison with *G* beams. A higher transmittance (*T*) of LG beams was observed in the diffusive region compared with the *G* beam.

The schematic diagram of the experimental setup is shown in Fig. 1. A He–Ne laser of 5 mW at 633 nm was used as a light

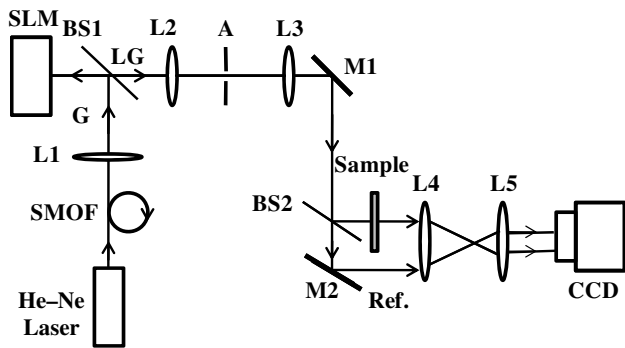


Fig. 1. Experimental setup where SMOF is a single-mode optical fiber; L are lenses; G is the Gaussian beam; BS is a beam splitter; SLM is a spatial light modulator; LG is the Laguerre–Gaussian beam; A is the aperture; M are mirrors; and CCD is a charge coupled device camera.

source. The beam output from the laser was focused into a single-mode optical fiber (SMOF). The output beam from the SMOF was used to illuminate a spatial light modulator (SLM, HoloEye LC-R 720) working in the reflection mode. The LG beams with different OAM states were generated using the SLM with different forked diffraction patterns. The generated LG beams were then divided by a beam splitter into two separate beams used as sample and reference beams, respectively, as shown in Fig. 1. A sample cell containing scattering medium was placed in the path of the sample beam. The reference beam not passing the scattering medium was used, as in conventional transmittance measurements, to monitor and take into account the change of incident light power and avoid the effect of fluctuation of the incident light power to the T calculation. The images of the sample beam output from the turbid media and the reference beam were recorded simultaneously using the same 16-bit CCD camera (Photometrics CH250L, 512×512 pixels). The transmittances of light in the different scattering media were calculated based on the ratio of the intensity of the sample beam image over the intensity of the reference beam image.

The SLM diffraction patterns and the corresponding LG beam shapes used in this study are shown in Fig. 2. The forked diffraction patterns were created using a MATLAB-based software (HoloEye SLM application software). The forked diffraction patterns correspond to interference patterns of a TEM_{00} beam and a LG_0^L beam. Therefore, when a TEM_{00} Gaussian beam is used to illuminate the different forked diffraction patterns in SLM, the LG beams with different values

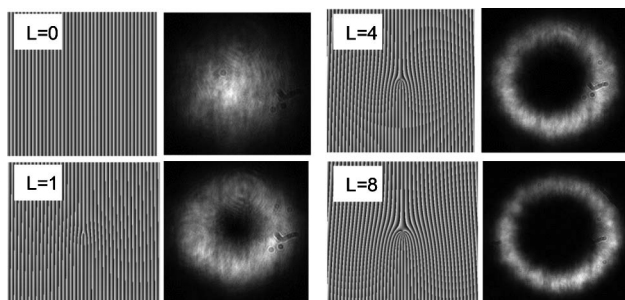


Fig. 2. HoloEye SLM diffraction patterns and corresponding generated LG beams.

of L will be generated, which have helical and twisted wavefronts.

The scattering media used in the experiments were made with various sizes and concentrations of polystyrene latex microspheres (beads) in water solutions. The thicknesses (z) of the turbid media were varied to study the transmittance of LG beams as a function of the ratio of sample thickness to the scattering mean free path (l_s) of the media, i.e., T versus z/l_s . The z/l_s is the number of scattering events happening in the turbid medium in length z . Two types of beads with diameters of $0.107 \mu\text{m}$ and $3.12 \mu\text{m}$ were used as typical small and large scattering particles compared with the wavelength of light, respectively, to study the effect of particle size on the scattering and transmission of LG beams. The concentration of the scattering media is 1% diluted from the commercial bead solution (10% in stock).

The scattering mean free path l_s , the transport mean free path l_{tr} , and the anisotropic factor g as a function of particle size and wavelength for 1% of the polystyrene latex bead solutions (10% in stock) have been investigated elsewhere [6]. Using Ref. [6], the values of l_s , l_{tr} , and anisotropic factor g at 633 nm for the 1% concentration turbid medium consisting of $d = 0.107 \mu\text{m}$ small bead particles were estimated as $l_s = 500 \mu\text{m}$, $l_{tr} = 500 \mu\text{m}$, and $g = 0$, respectively. In contrast, the values of l_s , l_{tr} , and g at 633 nm for the 1% concentration turbid medium consisting of $d = 3.12 \mu\text{m}$ large bead particles were estimated as $l_s = 100 \mu\text{m}$, $l_{tr} = 800 \mu\text{m}$, and $g = 0.875$, respectively.

The received signal beam images of the G and LG beams with $L = 0, 1, 4$, and 8 were recorded for both small and large bead solutions with fourteen (14) thicknesses of the turbid media varied in a wide range from 0 to 40 mm (i.e., $z = 0, 0.1, 0.2, 0.5, 1, 2, 3, 4, 5, 6, 8, 10, 20$, and 40 mm) covering all of the ballistic and diffusive regions. Due to the page limit, it is hard to show all of the recorded images in this Letter. As examples, Fig. 3 shows part of the received sample beam images of the G beam ($L = 0$) and the LG beam with $L = 4$ through the scattering medium consisting of small bead particles ($d = 0.107 \mu\text{m}$) with $z/l_s = 0, 1, 2, 6, 10, 12, 16$, and 20 (corresponding to $z = 0, 0.5, 1, 3, 5, 6, 8$, and 10 mm). It can be seen from Fig. 3 that as thickness increases, the intensity of the recorded images of the G and LG beams decreases and images become more diffuse.

Similar image features shown in Fig. 3 were observed for the scattering media consisting of large bead particles ($d = 3.12 \mu\text{m}$).

Based on the recorded images data, the transmittances T of the LG and G beams in scattering media with different particle sizes, sample thicknesses, and OAM values L were calculated using the following five major steps: (1) for each scattering solution, a sample thickness (z/l_s), and an LG beam with a specific OAM value L , take a ratio of the intensity of the received sample beam image (I_S) over the intensity of the reference beam image (I_R) recorded with scattering media in the sample beam path, and mark the ratio as $A = (I_S/I_R)_{\text{with sample}}$; (2) take a background ratio of I_S over I_R recorded without the scattering media sample, mark the ratio as $B = (I_S/I_R)_{\text{no sample}}$, and use B as a calibration ratio; (3) calculate T defined as $T = A/B$; (4) using a similar method to calculate T for other images recorded with different L , z/l_s , and solutions. In all T calculations, the same wide image areas, and

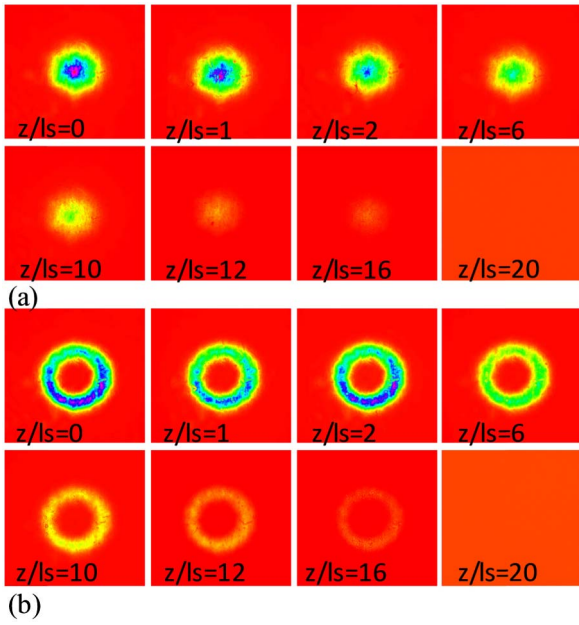


Fig. 3. Recorded images of (a) the Gaussian beam ($L = 0$) and (b) LG beam with $L = 4$ through a scattering medium consisting of small bead particles ($d = 0.107 \mu\text{m}$) at different thickness of $z/l_s = 0, 1, 2, 6, 10, 12, 16,$ and 20 .

therefore the same numbers of CCD pixels were used for both the LG and G beams and for both the reference and sample beam images; and (5) plot T versus z/l_s , or $\text{Log}T$ versus z/l_s for different L and solutions with different scattering particle sizes.

Figure 4 shows $\text{log}T$ as a function of ratio z/l_s and topological charge L of LG beams for the scattering media consisting of small particles ($d = 0.107 \mu\text{m}$) in a 1% concentration solution (volume density) of the commercial bead solution (10% in stock). The following four salient features can be seen from Fig. 4: (1) within the ballistic region, where z/l_s is small and ballistic transition is the dominant process, the LG and G beams show no significant differences in transmittance defined as above ($T = A/B$). The transmittance differences of the LG and G beams in this region are small, randomly changed, and within the experimental errors; (2) within the diffusive region,

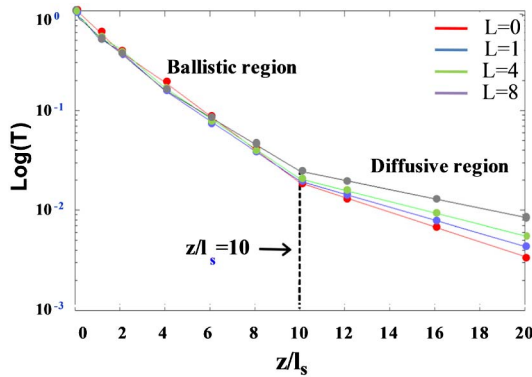


Fig. 4. $\text{Log}T$ as a function of z/l_s , where z is the thickness of turbid media and l_s is the scattering mean free path of the turbid medium (beads in water, $d = 0.107 \mu\text{m}$, $l_s = 500 \mu\text{m}$).

where z/l_s is large and multiple scattering is the dominant process, the LG beams show a higher received signal than the G beams; (3) within the diffusive region, the LG beams with larger L values show a higher received signal than the LG beams with small L values; and (4) the transition point from the ballistic region to the diffusive region [7,8] for this small particle solution was observed at $z/l_s = 10$. The reason behind the change of decay slopes of $\text{log}T$ in the ballistic and diffusive regions has been well studied and understood [6–8]. In the ballistic region, nonscattered light dominates and attenuation falls exponentially by Beer’s law. In the diffusive region, multiple scattered light dominates, which slows the rate of attenuation, resulting in a higher received signal level than for the ballistic slope.

Figure 5 shows $\text{log}T$ as a function of z/l_s and a topological charge L of LG beams for the turbid media consisting of large particles ($d = 3.12 \mu\text{m}$) in a 1% concentration solution of the commercial bead solution (10% in stock). In order to compare with Fig. 4, a semi-logarithmic scale was used in Fig. 5. The following similar features can be seen from Fig. 5: (1) LG and G beams show no significant differences of transmittance in the ballistic region; (2) LG beams show a higher T than the G beams in the diffusive region; and (3) the LG beams with larger L values show a higher T than the LG beams with small L values in the diffusive region. However, the transition point from the ballistic to the diffusive regions for the large particle solution was observed at $z/l_s = 94$, which shows a significant difference from that observed for the small scattering particles.

The difference of the transition points from the ballistic to the diffusive regions for the small and large particle solutions is caused by their different scattering parameters such as scattering mean free path l_s , and transport mean free path l_{tr} . Using the values of $l_s = 500 \mu\text{m}$, $l_{tr} = 500 \mu\text{m}$, and $g = 0$ for the $d = 0.107 \mu\text{m}$ bead solution, and $l_s = 100 \mu\text{m}$, $l_{tr} = 800 \mu\text{m}$, and $g = 0.875$ for the $d = 3.12 \mu\text{m}$ bead solution, the observed transition points from the ballistic to the diffusive regions, $z/l_s = 10$ for the small particles, and $z/l_s = 94$ for the large particles can be indicated as the terms of z/l_{tr} . The transition points will become $z/l_{tr} = 10$ for the small particles and $z/l_{tr} = 12$ for the large particles. Although the values of the transition points in terms of z/l_s for the small

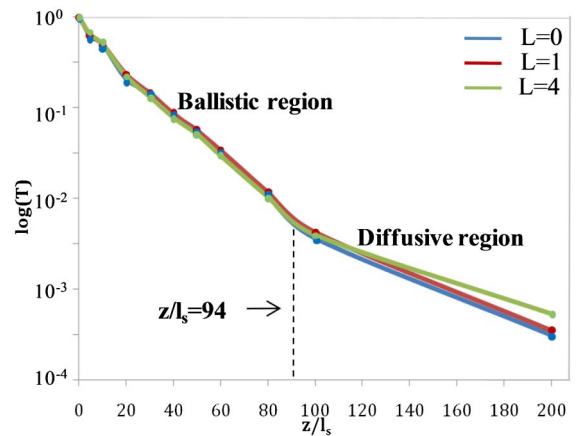


Fig. 5. $\text{Log}T$ as a function of z/l_s , where z is the thickness of turbid media and l_s is the scattering mean free path of the turbid medium (beads in water, $d = 3.12 \mu\text{m}$, $l_s = 100 \mu\text{m}$).

Table 1. Comparison of l_s , l_{tr} , g , and Transition Points for $d=0.107\ \mu\text{m}$ and $d=3.12\ \mu\text{m}$ Bead Solutions

Comparing Items	Small Particles	Large Particles
Particle size d (μm)	0.107	3.12
L_s (μm)	500	100
L_{tr} (μm)	500	800
G	0	0.875
Transition point at z/l_s	10	94
Transition point at z/l_{tr}	10	12

and large particles show remarkable differences, the values of the transition points in terms of z/l_{tr} are closed. These results are in good agreement with the results obtained from time-resolved measurements and calculations using Mie theory by Yoo *et al.* [9]. Their results show that diffusive approximation is valid only when $z/l_{tr} \geq 10$ for both small and larger particles. The transition points of $z/l_{tr} = 10$ for the small particles and $z/l_{tr} = 12$ for the large particles observed in our experiments satisfy the criterion of $z/l_{tr} \geq 10$. Table 1 summarizes and compares the parameters of l_s , l_{tr} , g , and the transition points from ballistic to diffusive regions for the small and large bead solutions used in this study.

Our experimental results show that, within the diffusive region, the LG beams show a higher received signal than the G beams, and the LG beams with higher L values show a higher received signal than the LG beams with lower L values. These differences of the received signal levels may arise from the different beam structures and the vortex nature of LG beams. Because the received signal beam intensity recorded in the CCD camera includes contributions from both ballistic and forward scattered photons, and the ballistic component is very weak in the diffusive region, the observed higher received signal of LG beams may show different forward scattering for LG and G beams. Since the spatial anisotropy of scattering is mainly given by anisotropy factor g , the different forward scattering feature of LG and G beams in turbid media may indicate their different g values, which may alter the spatial distribution of scattering events in a way that results in more scattering light staying close to the beam axis, and hence collected by the CCD camera.

Several groups reported their theoretical and simulation studies on the scattering of focused LG beams in turbid media [3,4]. Ou's group calculated the scattering of LG beams by homogeneous spheroids based on the generalized Lorenz–Mie theory [4]. Their simulation results show that the magnitude of the scattering intensity decreases as the topological charge L increases. They explained this decrease by the higher-order vortex beams having larger central dark areas that may interact less with scattering particles in the turbid media, yielding less scattering [4]. Sun's group focused their study on the tightly focused vortex beams through turbid media based on the Monte Carlo calculation. They also did preliminary transmission measurements on inhomogeneous scattering media samples consisting of corroded glass slabs, and obtained the following differential results: the transmission of LG beams

in turbid media is higher than for G beams for tightly focused beams, while the transmission of LG beams in turbid media is smaller than for G beams for the slightly focused beams [3]. In contrast, our work shows the systematic experimental study for the scattering and propagation of nonfocused LG vortex beams in typical homogeneous scattering media, and consistently observed differences in the received signal levels of LG and G beams, which should be more generally of interest and useful for light propagation and imaging studies of complex beams.

It is important to establish a physical model to study the scattering difference of LG and G beams in turbid media. However, to the best of our knowledge, there is a lack of such studies to reveal the underlying physics and establish a basic simulation model to understand the scattering differences of LG and G beams. We expect our observation to stimulate more theoretical and experimental studies to investigate and clarify the effect of vortex structures of complex beams on the light scattering and imaging in turbid media, and evaluate imaging efficacy of LG beams for deep target detection in scattering media. We will study eigen channels of the transmission matrix in the diffusive region for the propagation of complex light in turbid media and investigate if the vortex structure and helical wavefronts of LG beams can form a subset of eigen modes to better travel through eigen channels in scattering media [10,11]. In addition, we plan to investigate the effect of vector beam structures of complex light to the scattering and imaging in turbid media with different experimental conditions and simulation algorithms in collaboration with theoretical groups.

Funding. Army Research Office (ARO) (W911NF-13-1-0151).

Acknowledgment. We thank Giovanni Milione and Thien An Nguyen for their help during the initial stages of the work.

REFERENCES

1. D. Palacios, D. Rozas, and G. A. Swartzlander, Jr., Phys. Rev. Lett. **88**, 103902 (2002).
2. H. Sztul, "Optical vortices: Angular momentum of light, energy propagation and imaging," Ph.D. thesis (City University of New York, 2008).
3. C. Z. Sun, Z. Y. Chen, and J. X. Pu, Acta Opt. Sin. **34**, 0601002 (2014).
4. J. Ou, Y. S. Jiang, Y. W. Shao, X. S. Qu, H. Q. Hua, and D. H. Wen, Acta Phys. Sin. **62**, 114201 (2013).
5. M. Luo, Q. Chen, L. Hua, and D. Zhao, Phys. Lett. A **378**, 308 (2014).
6. R. R. Alfano, W. B. Wang, L. Wang, and S. Gayen, *Photonics, Volume IV: Biomedical Photonics, Spectroscopy, and Microscopy*, D. Andrews, ed. (Wiley, 2015), p. 367. Chap. 9.
7. M. Kempe, A. Z. Genack, W. Rudolph, and P. Dorn, J. Opt. Soc. Am. A **14**, 216 (1997).
8. L. Shi, L. A. Sordillo, A. Rodriguez-Contreras, and R. R. Alfano, J. Biophoton. **9**, 38 (2016).
9. K. M. Yoo, F. Liu, and R. R. Alfano, Phys. Rev. Lett. **64**, 2647 (1990).
10. S. M. Popoff, G. Lerosey, R. Carminati, M. Fink, A. C. Boccara, and S. Gigan, Phys. Rev. Lett. **104**, 100601 (2010).
11. J. Baumgartl, T. Cizmar, M. Mazilu, V. C. Chan, A. E. Carruthers, B. A. Capron, W. McNeely, E. M. Wright, and K. Dholakia, Opt. Express **18**, 17130 (2010).